Facile synthesis of reduced graphene oxide by *Tecoma stans* extracts for efficient removal of Ni (II) from water: batch experiments and response surface methodology

Alaa El Din Mahmoud[1,2]* ⬥, Mohamed Hosny[1,2], Nourhan El-Maghrabi[1,2] and Manal Fawzy[1,2,3]

Abstract

A facile approach to synthesize reduced graphene oxide (rGO) was investigated using three different extract concentrations of *Tecoma stans* leaves as reducing/capping agents. The surface morphology of the rGOs was examined by scanning electron microscopy with energy dispersive X-ray. The optimum prepared rGOs were confirmed with characteristic peaks at ∼ 280 nm using UV–Vis Spectroscopy. Fourier-transform infrared spectroscopy results indicated the capacity of plant extracts to reduce the oxygen functional groups on graphite oxides' surfaces. Furthermore, the organic constituents of the plant extract were determined to highlight the reduction mechanism of graphene oxide to rGO. The optimized rGO was subsequently utilized as an adsorbent for the removal of Ni (II) from simulated wastewater. Adsorption experiments were conducted using methods of one factor at a time as well as Box Behnken Design. The Ni (II) adsorption is fitted well to the non-linear isotherm models and the calculated maximum uptake capacity was 69 mg g^{-1}. The optimum removal of Ni (II) was found 93% with pH of 6, initial Ni (II) concentration of 2 mg L^{-1}, and rGO dose of 0.2 g L^{-1}. The reliability of the developed model was 99.4% between experimental and predicted values. In addition, the average desorption efficiency of Ni (II) was 94%, which highlight the applicability of rGO reusability.

Keywords: rGO, Yellow elder plant, Green synthesis, Uptake capacity, Nickel, Water, Models, Kinetics, Box–Behnken design, Desorption

1 Introduction

Water pollution with poisonous heavy metals has short- and long-term impacts on the environment as well as human-beings. This is due to their persistence, toxicity even at low concentrations, and bioaccumulation/biomagnification in the food web [1]. The exposure of non-essential heavy metals to aquatic organisms and humans can be through various routes. For instance, inhalation, ingestion, and absorption [2].

In 2025, it is expected that the volume of wastewater effluents comprising organic/inorganic contaminants will be doubled compared to 2010. One of the frequent detected heavy metals in industrial wastewater is nickel. The maximum allowable limits of Ni (II) are 2.0 mg L^{-1} in industrial wastewater and 0.01 mg L^{-1} in drinking water, according to the World Health Organization. However, various ranges of Ni (II) concentrations are present in various industries including the effluents of steel, petroleum, electroplating, batteries, and pigments manufacturing [3]. Consequently, it is vital to develop a sustainable and cost-effective treatment process to

* Correspondence: alaa-mahmoud@alexu.edu.eg
[2]Green Technology Group, Alexandria University, Alexandria 21511, Egypt
Full list of author information is available at the end of the article

Mahmoud *et al. Sustainable Environment Research*   (2022) 32:22

Page 2 of 16

reduce/prevent the direct discharge of heavy metals especially Ni (II) into the water bodies. The demand of Ni is growing, and its price reached USD 20.3 kg^{-1}.

Herein, adsorption process was proposed as an alternative route to the existing wastewater treatment techniques. Adsorption is the process of a substance being retained or transferred from an aqueous solution to the solid phase [4]. Unlike techniques as precipitation, electroplating, coagulation, and membrane separation, adsorption is an eco-friendly and promising technique for heavy metals removal [5, 6]. It is a convenient technique with the advantage of easy operation, cost-effective, and no byproduct formation. The successful application of adsorption process depends on using the suitable sorbents.

Graphene based (nano-)materials have fast sorption kinetics for metal ions beside their high stability due to the graphene structure with opened-up layer [7]. Due to the unique properties and characteristics of graphene, the synthesis of either graphene or its derivatives are promising especially with green chemistry principles. The common approach for the production of reduced graphene oxide (rGO) is the chemical exfoliation through the oxidation of graphite and the graphene oxide reduction process [8]. The employed hazardous reducing agents are sodium borohydride (NaBH$_4$), hydroquinone (C$_6$H$_6$O$_2$), hydrazine (N$_2$H$_4$·H$_2$O), dimethylhydrazine (C$_2$H$_8$N$_2$), and hydrogen sulfide (H$_2$S). However, the large-scale and real application of the prepared rGO with toxic reducing agents is harmful and hazardous to the environment and human [9].

As an alternative route of reduction process, eco-friendly and scalable approaches are adopted using green reducers extracted from plant biomass since they are noncorrosive and inexpensive. Plant extracts have the potential to reduce graphene oxide due to the presence of various phytochemicals constituents according to the type of the plant biomass. In this research, *Tecoma stans* leaves extract has been used as a reducing agent for graphene oxide for the first time to substitute the toxic chemical agents. *T. stans* is a worldwide ornamental species in Africa, Asia, and Oceania, especially tropical and subtropical countries [10].

There is little literature investigating *T. stans* extracts in the preparation of metallic nanoparticles. For instance, Hariram et al. used the *T. stans* flower extract for the preparation of nano silver-talc and its application in antimicrobial [11]. Recently, a study dedicated on the biosynthesis of nano magnesium oxide (MgO) using the extracts of flower, bark, and leaf of *T. stans* to be utilized in the treatment of dyes [12]. Therefore, in this research, *T. stans* leaves extract was utilized for the first time in the phytosynthesis of rGO under different synthetic conditions. Subsequent to the green synthesis procedure, the prepared rGOs were characterized and the optimized rGO was utilized for Ni (II) removal using both batch and statistically designed experiments.

One of the useful tools in the statistical design is response surface methodology (RSM). The effects of several factors can be investigated by RSM with minimum number of batch experiments compared to one factor at a time separately. Consequently, Box-Behnken Design (BBD) was adopted using the investigated process factors to optimize Ni (II) removal from simulated wastewater. BBD is considered as a global design which is more economic than other designs regarding the number of conducted experiments with three levels.

2 Materials and methods

Graphite powder (98% Extra pure) was obtained from LOBA CHEMIE India. Hydrochloric acid (HCl) (37%), nitric acid (HNO$_3$), sodium hydroxide (NaOH) powder, sulfuric acid (H$_2$SO$_4$), potassium permanganate (KMnO$_4$) and standard Ni (II) solution were purchased from Sigma Aldrich, USA. While hydrogen peroxide (H$_2$O$_2$) and sodium nitrate (NaNO$_3$) were purchased from PIOCHEM, Egypt and ISO-CHEM, France, respectively.

2.1 Graphene oxide (GO) synthesis

The GO was synthesized using the modified Hummer method. A total of 1 g of graphite powder, 100 mL of 98% H$_2$SO$_4$, and 1 g of sodium nitrate (ISO-CHEM) were placed in a flask and stirred for 15 min, then 6 g of KMnO$_4$ was gradually added within 10 min. During KMNO$_4$ addition, the temperature was kept below than 10 °C to ensure homogenous GO. The reaction mixture was stirred at 35 °C overnight then 50 mL of deionized water (DI) was gently added, raising the temperature to roughly 90 °C under stirring for 1 h.

Finally, 140-mL of DI was added, followed by 10-mL of H$_2$O$_2$. Consequently, GO (brownish yellow) was formed. Afterwards dry GO was attained by washing for multiple cycles using HCl first then water and centrifugation at 5000 rpm for 10 min and drying at 45 °C for 3 d. Furthermore, sonication of GO in DI was used to achieve exfoliation using bath sonicator (FALC, LABSONIC LBS2, Italy) for 1 h, generating a well dispersed GO.

2.2 Preparation of plant extracts

Leaves of *T. stans* (denoted as X) were collected from the North Coast of Alexandria City (30°57′43.6″ N 29°32′32.1″ E). X biomass was washed with water to eradicate any dust, or any other contaminated particles then washed many times with DI and dried at 50 °C till the weight became constant. The dried biomass was pulverized in a stainless-steel mixer.

Three different weights of X biomass (500, 2500, and 5000 mg) were added to 100 mL of DI representing concentrations of 5, 25, and 50 mg mL^{-1}, respectively. Each mixture was stirred at room temperature for 90 min with a stirring rate of 400 rpm (magnetic stirrer; FALC, F91T, Italy) then filtered using Whatman 8 µm filter paper.

2.3 Green synthesis route for reduced GO (rGO)
Firstly, 0.1 g of GO powder was added in 100 mL of DI. The solution was sonicated for about 1 h. Consequently, a brown color homogeneous dispersion of GO was obtained.

For the reduction process, 50 mL of *T. stans* extracts (prepared with different concentrations) were added to 50 mL of 1 mg mL^{-1} GO then the mixture was stirred and heated at 70 °C for 12 h. Afterwards the brownish color of dispersed GO converted to a black colored solution. The obtained solutions were centrifuged at 5000 rpm and washed three times with DI. Furthermore, product was dried at 60 °C overnight and designated to be rGO-X-5 or rGO-X-25 or rGO-X-50 according to the concentration of *T. stans* (X).

2.4 Characterization
UV-Vis spectroscopy was analyzed for the prepared GO and rGO suspensions (1 mg mL^{-1}) after 30 min of ultrasonication. Subsequent to the preparation of the suspensions, they were diluted to assure translucency prior of the measurements using a Spectrophotometer (PG Instruments T80+, UK). A scanning electron microscope (SEM; JOEL-JSM-IT200) with an energy dispersive X-ray spectroscope (EDX) was utilized to examine the surface morphologies of the samples. The prepared samples for SEM were coated with gold using ion sputter evaporator (JFC-1100E-JOEL). Fourier-transform infrared (FT-IR) spectra were measured by Cary 630 (Agilent Technologies, Germany) with attenuated total reflectance at 4 cm^{-1} resolution.

2.5 Gas chromatography-mass spectrometry (GC-MS)
The phytochemical composition of *T. stans* leaves extract was detected and analyzed. Further details are illustrated in the Supplementary Materials.

2.6 Batch experimental models
A simulated wastewater containing 100 mg L^{-1} of Ni ions (stock solution) was prepared by dilution of factor 10 with DI. Firstly, the effect of contact time and pH was investigated by one factor at a time (OFAT) method at different Ni (II) concentrations. The initial experiments were conducted up to 60 min. pH values were adjusted to be in the range of (3–6) using 0.1 M HCL and 0.1 M NaOH. Furthermore, two different doses were chosen to be utilized in the abovementioned

experimental work: 2 and 6 mg of rGO-X-25. All samples before and after the treatment were diluted with a dilution factor of 10 with DI. Eventually, all the samples were preserved by adding just few drops of very diluted nitric acid (0.001 M HNO$_3$) and then stored at 4 °C until the measurement of Ni concentrations was conducted using Atomic Absorption Spectroscopy (ContrAA 300, Germany). The experimental results were found reproducible when the experiments were conducted in triplicates.

The removal efficiency (R) and the uptake capacity (q$_t$) of Ni (II), using rGO-X-25, were calculated using Eqs. (1) and (2) [13, 14].

$$q_t = \frac{C_0 - C_t}{m} \ x \ V \ , \tag{1}$$

$$R = \frac{C_0 - C_t}{C_0} \ x \ 100 \ , \tag{2}$$

where q$_t$: the uptake capacity (mg g^{-1}), C$_0$: initial concentration (mg L^{-1}), C$_t$: concentration at time t (mg L^{-1}), R: removal percentage (%).

Isotherm models were analyzed using Langmuir, Freundlich, and Temkin models (Eqs. (3)–(5)). Furthermore, the separation factor (SF) is calcualted to indicate the feasibility of the adsorption process (Table 1; Eq. (6)). The prediction of adsorption rate is also investigated through the kinetic models; pseudo-first-order (PFO; Eq. ((7)) and pseudo-second-order (PSO; Eq. (8)). The nonlinear equations of the studied models are given in Table 1.

2.7 Optimization experiments: response surface methodology
Optimization experiments were based on RSM using BBD. Design Expert 11 was used to implement the models. Herein, the effect of three factors; pH, initial Ni (II) concentration, and rGO-25 dose were investigated on the removal percentage of Ni (II) as a response. The studied factors and their levels (low, medium, high levels; – 1, 0, + 1) are shown in Table 2. The independent parameters and the removal of Ni (II) efficiency response were demonstrated and optimized by analysis of variance (ANOVA). The number of experiments (N) in BBD was determined using Eq. (9).

$$N = 2k(k-1) + C_p, \tag{9}$$

where k: the number of factors and C$_p$: the central point's replicate number to estimate the pure error in the model considering the three levels of dose parameter with the central points of pH and Ni (II) concentration. All experiments were conducted in triplicate and the removal efficiency (R%) are obtained as average values.

Mahmoud *et al. Sustainable Environment Research*   (2022) 32:22

Page 4 of 16

Table 1 Isotherm and kinetic adsorption models

Adsorption models	Nonlinear equation	Parameters
Isotherm		
Langmuir; Eq. (3)	$q_e = \frac{q_m\,K_L\,C_e}{1+K_L\,C_e}$	q_e: the equilibrium loading of Ni (II) (mg g^{-1}), q_m: the maximum loading of Ni (II) per g of adsorbent (mg g^{-1}), K_L: constant of Langmuir equilibrium for the affinity between the adsorbent and Ni (II) (L mg^{-1}).
Freundlich; Eq. (4)	$q_e = K_f\,C_e^n$	K_f: constant of Freundluch for the adsorption strength ((mg g^{-1}) (mg L^{-1})^n), n: the adsorption intensity
Temkin; Eq. (5)	$q_e = B\ln(K_T\,C_e)$	B: the adsorption heat constant (J mol^{-1}); B= $\frac{R_T}{b}$, R: gas constant (8.314 J mol^{-1} K^{-1}), T: temperature (K), and K_T: constant of Temkin binding (L mg^{-1}).
Separation factor; Eq. (6)	$SF = \frac{1}{1+K_L C_0}$	SF: Separation factor (dimenstionless), C_0: initial adsorbate concentration (mg L^{-1}).
Kinetic		
pseudo-first-order; Eq. (7)	$q_t = q_e\,(1-\exp(-k_1\,t)$	k_1: PFO constant rate (min^{-1}), t: contact time (min).
pseudo-second-order; Eq. (8)	$q_t = \frac{q_e^2\,k_2\,t}{1+k_2 q_e\,t}$	k_2: PSO constant rate (g mg^{-1} min^{-1}).

The established model type is polynomial, and this model correlates the relationship between the investigated factors and the response (R). It can be expressed by Eq. (10).

$$R = \beta_0 + \beta_1 X_1 + \beta_2 X_2 + \beta_3 X_3 + \beta_{12}X_1X_2 + \beta_{13}X_1X_3 + \beta_{23}X_2X_3 + \beta_{11}X_1^2 + \beta_{22}X_2^2 + \beta_{33}X_3^2, \quad (10)$$

where Xi: the investigated factors (pH, Ni (II) initial concentration, and rGO-X-25 dose), β_0: constant coefficient (intercept), $\beta_1/\beta_2/\beta_3$: Linear coefficients show the main effect of each factor, $\beta_{12}/\beta_{13}/\beta_{23}$: Interaction coefficients demonstrate the interaction effect between two variables, $\beta_{11}/\beta_{22}/\beta_{33}$: Quadratic coefficients indicate the shape of the curve.

Furthermore, the significance and suitability of the designed model were assessed by the determination/regression coefficient (R^2; Eq. (11)) and corrected determination/regression coefficient (Adj R^2; Eq. (12)).

$$R^2 = 1 - \frac{SS_{residual}}{SS_{model} - SS_{residual}}, \quad (11)$$

$$Adj\,R^2 = 1 - \frac{SS_{residual}/DF_{residual}}{(SS_{model} + SS_{residual})/\left(\frac{DF_{model}}{DF_{residual}}\right)}, \quad (12)$$
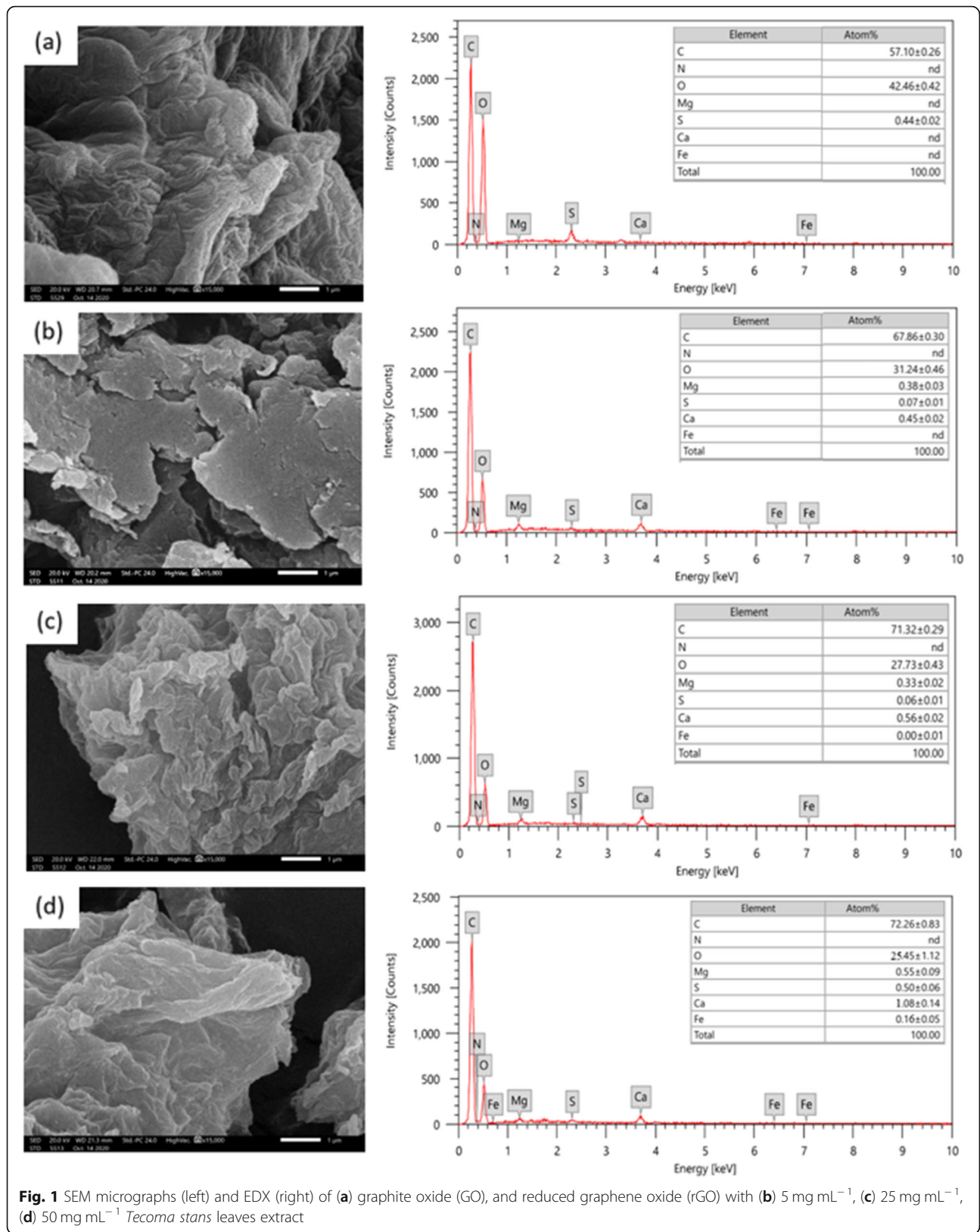
where SS: sum of squares and DF: degree of freedom.

3 Results and discussion

3.1 The surface morphologies

Figure 1a illustrates the wavy and coarse wrinkled features of the prepared GO. This is due to the surface agglomeration resulting from the oven-drying of the product and the breakage of the bond conjugated in the precursor graphite powder during the synthesis procedure. It is noticeable that the surface morphologies of rGOs are quite different when prepared with different plant extract concentrations. Figure 1b reveals that rGO-X-5 arranged as stacked several layers as sheets via Van-der Waals interactions and this finding is similar to Ansari et al. [15]. With increasing the plant extract concentration from 5 to 25–50 mg mL^{-1}, Fig. 1c and d demonstrates corrugated and wrinkled shape for rGO-X-25 and rGO-X-50.

The elemental analysis of GO and the synthesized rGOs samples was detected by EDX. EDX could approximate the elements composition. Figure 1a shows the O:C ratios of the used precursor of GO was 0.74. This ratio is always variable according to the synthesis procedure and its condition of GO. Neolaka et al. [16] reported the O:C ratio of GO (modified hummers method) being 0.65. The O:C ratios of the prepared rGOs were dramatically decreased after the reduction procedure in the following order: rGO-X-5 (0.46) > rGO-X-25 (0.38) > rGO-X-50 (0.35) (Fig. 1). These findings indicate the successful application of *T. stans*

Table 2 Experimental factors and levels used for the optimum Ni (II) removal onto rGO-X-25

Factors (Independent variables)	Units	Levels		
		-1	0	+1
pH	(—)	3	4.5	6
Ni (II) initial concentration (Conc.)	(mg L^{-1})	2	6	15
rGO-X-25 dose (Dose)	(g L^{-1})	0.06	0.13	0.20

Fig. 1 SEM micrographs (left) and EDX (right) of (**a**) graphite oxide (GO), and reduced graphene oxide (rGO) with (**b**) 5 mg mL^{-1}, (**c**) 25 mg mL^{-1}, (**d**) 50 mg mL^{-1} *Tecoma stans* leaves extract

extract as reducing and capping agent for the removal of oxygen functional groups.

3.2 Spectroscopy analysis

Figure 2a shows the UV-Vis spectra of GO and rGO with different concentrations of *T. stans* extract. The spectrum of GO showed an absorbance peak at 230 nm which ascribed to the π–π* transition of C=C. The presence of an absorbance peak in the range of 230–240 nm is the characteristic peak of GO according to Mahmoud [8] and Emadi et al. [17]. The n–π* transitions of C=O

(carbonyl groups) could be responsible for the small shoulder (335 nm). It is noted that the absorbance peaks of rGO-X-25 and rGO-X-50 were shifted to ~ 280 nm subsequent to the GO reduction. The plasmon peaks shift reveals the decreasing of the oxygen functional groups (i.e., carboxyl groups) [18].

FT-IR spectra analysis are shown in Fig. 2b to recognize the probable functional groups of the phyto-constituents present in *T. stans* biomass, GO, and the yield products of rGO by three different concentrations of *T. stans* extracts (5, 25, and 50 mg mL^{-1}). -OH band
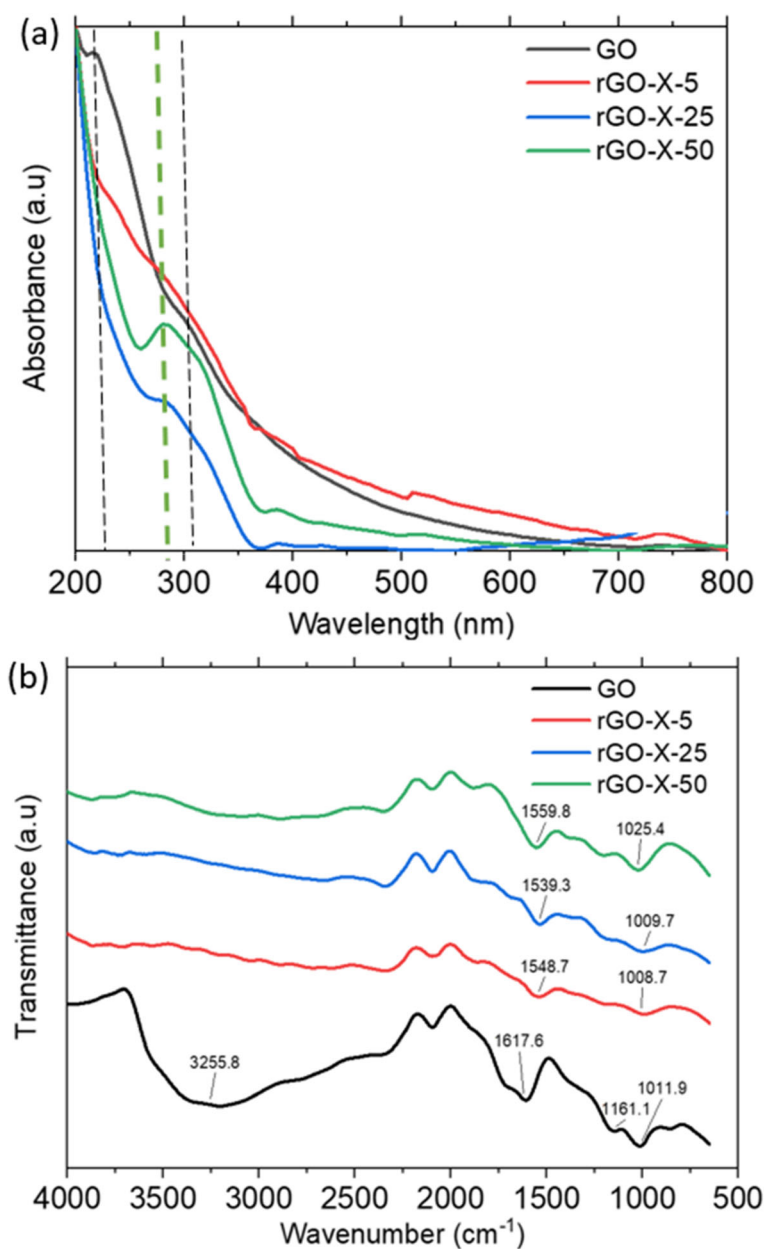

Fig. 2 (**a**) UV–Vis spectroscopy and (**b**) FT-IR spectra of graphene oxide (GO), and reduced graphene oxide (rGO) using different concentrations of *Tecoma stans* leaves extract (5, 25, and 50 mg mL^{-1} of leaves extract)

appeared at 3255.8 cm^{-1} in IR spectra of GO. This band is completely disappeared for the three rGOs confirming the successful reduction of GO to indicate the maximum decrease of hydroxyl groups within the graphitic sheets. These findings are consistent with those of Vatandost et al. [19] and Ding et al. [20].

In GO, the band of C=C is recorded at 1617.6 cm^{-1} which is similar to the result obtained by Kurmarayuni et al. [21]. Subsequent to the reduction of GO, this band is shifted to lower wavenumber. C-O of ether group is disappeared in the rGOs spectra which were detected in GO at 1161.1 cm^{-1}. Additionally, the intensity of C–O (epoxy group) that appeared in GO spectrum at 1011.9 cm^{-1} decreased in the three rGO samples. It is worth mentioning that the intensity of most peaks was lowered indicating the prepared rGOs have meaningfully less oxygen functional groups than GO and this is in line with Mahmoud [8]. The results of the current investigation are in accordance with other research works [22, 23].

The results of FT-IR spectra could conclude that phytochemicals in the aqueous plant extract possess a robust possible for reducing GO to rGO, which might be harnessed as a cost-effective and an efficient route to produce rGO on a large scale.

3.3 Reduction mechanism: phytochemistry

The results of GC-MS profile (Fig. S1) show the presence of different compounds which may be tangled in the green GO reduction. The retention times and mass-to-charge ratios (*m/z*) were used to identify 17 biomolecules. Table 3 illustrates the identified phytochemicals found in the studied plant extract with each retention time and their percentage. The major compounds are 1,10-Decanediol (61.5%), 2-Pentadecanone, 6,10,14-trimethyl (8.20%), E-10-Pentadecenol (5.33%), Neophytadiene (4.00%), Hexadecanoic acid, ethyl ester (3.24%), Phytol (1.96%), Isoquinoline (1.74%), and 3′,4′,7-Trimethyl quercetin (1.25%) according to their percentage order. The detected phytochemical compounds belong to volatile oils, fatty acids, isopernoidal ketone, terpenoids, flavonoids, and alkaloids. Larbie et al. [24] detected alkaloids, flavonoids, Coumarins, tannis constituents in the leaf extract of *T. stans*. These organic phytochemicals possess a role during the rGO synthesis directly and/or act as capping agents on rGO [25].

3.4 Heavy metals removal
3.4.1 OFAT

The uptake quantity and removal of Ni (II) on the optimized synthesized rGO (rGO-X-25) increased with raising the contact time during the first 15 min. Afterwards, the equilibrium is observed at 30 min (Fig. 3a and b). However, increasing the contact time revealed the occupation of the adsorption sites and saturation state was reached. Therefore, 30 min was considered as the optimum contact time in further experiments. Compared to literature studies, Ain et al. [26] found that the optimum contact time of magnetic graphene oxide was 25 min for Ni (II) adsorption. On the other hand, the uptake of Ni (II) on manganese ferrite-graphene oxide nanocomposite was fast in 50 min then reached the equilibrium at 270 min [27].
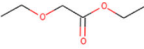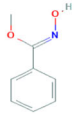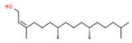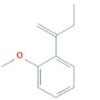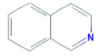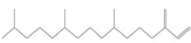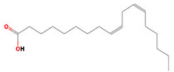
The q$_t$ decreased when the dose of rGO increased from 0.06 to 0.20 g L^{-1} as shown in Fig. 3c, while Fig. 3d shows the enhancement of Ni (II) removal. This behavior is attributed to the enhancement of rGO surface area which increased the availability of binding sites. rGO-X-25 was effective over a pH range of 3–6 (Fig. 3e). This pH range was selected because of the relative distribution of Ni species in the aqueous solutions as a function of pH. Fig. S2 illustrates that, at pH < 7, Ni (II) is the dominating species whereas at higher pH values its fraction decreased due to the formation of Ni hydroxides. Hence, the small difference in the heavy metal removal is probable due to the interactions of π–π as d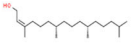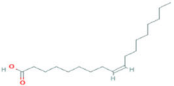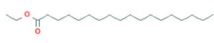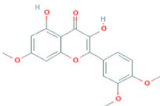ominant effects of between the adsorbents and the adsorbates [4]. Such behavior is advantageous for preparing these adsorbents for real application in wastewater with a pH that lies in this range [28, 29] and Ma et al. [30] confirmed that π-π interaction is one of the important mechanisms utilized in the toxic pollutant adsorption. π-π interaction of *Lactarius acerrimus* macrofungus cell wall with Hg (II) ions was concluded by Naeemullah et al. [31] to be the mechanism behind Hg adsorption. In addition, Eftekhari et al. [32] proved that the interaction of π-π possessed a major role in the removal of Cd^{2+} and Cu^{2+} by using Folic acid modified graphene oxide as they reported maximal adsorption capacities of 103 and 116 mg g^{-1} for Cd^{2+} and Cu^{2+}, respectively.

To investigate the changes of rGO-X-25 after the batch experiments, SEM-EDX was conducted, and the change of the adsorbent texture was observed and the appearance of Ni (II) peak in EDX analysis was detected which proves the occurrence of adsorption process (Fig. S3) compared to Fig. 1c.

3.4.2 Batch experimental models

Isotherm models are applied to demonstrate the affinity between the absorbent and the adsorbate when the adsorption process approaches equilibrium [5]. It is worth noting that, as shown in Fig. 4a, the q$_e$ increased with the increment of equilibrium concentration (C$_e$). This is due to the driving force that accelerates the pollutant diffusion onto the prepared rGO. The isotherm curves illustrate the type "L" shape without a strict plateau; no limited uptake capacity. Furthermore, it indicates that there is a high affinity from the adsorbate towards rGO.

Table 3 Identified phytochemical compounds found in the *Tecoma stans* extract using GC-MS

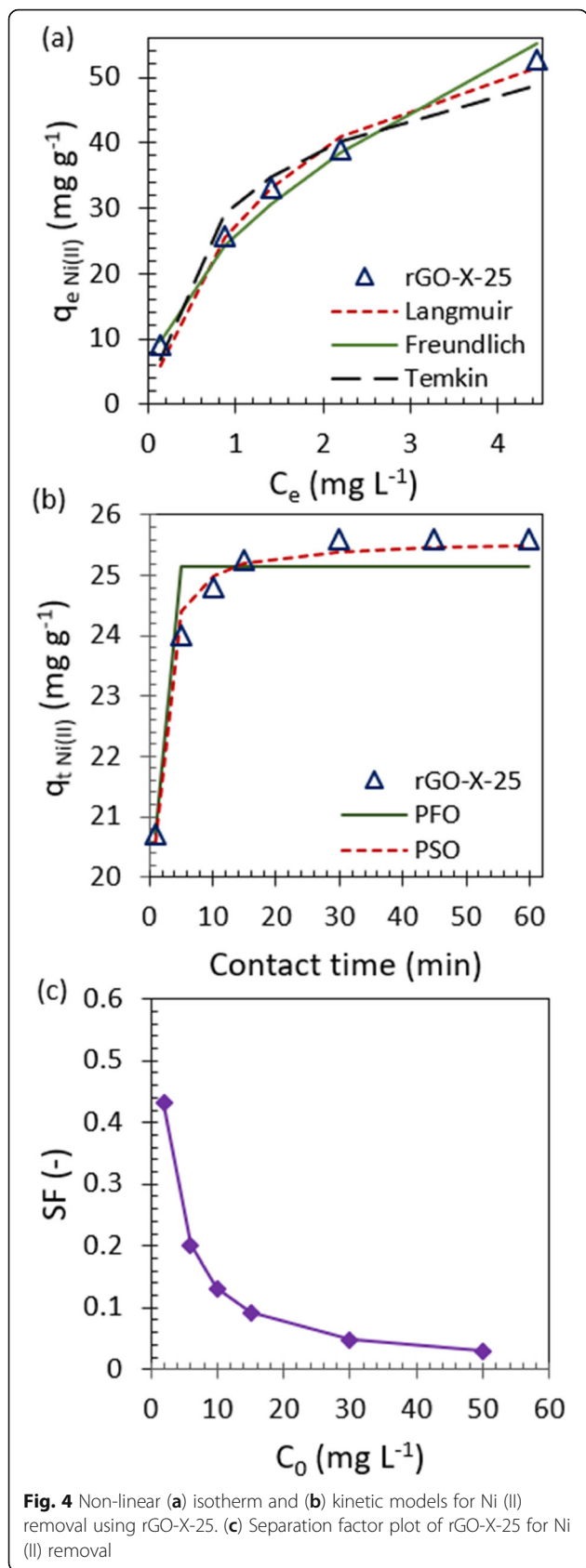| Compound name	Chemical structure	Category	Retention time (min)	Area (%)
Acetic acid, ethoxy-, ethyl ester		-	4.64	2.40
Methoxy ethoxy, phenyl-, oxime		Amino acid	5.02	1.32
Phytol		Terpenoids	17.07	1.20
Anisole, o-(1-ethylvinyl)		Ether	17.49	1.25
1,10-Decanediol		Fatty alcohols	18.89	61.5
E-10-Pentadecenol		Fatty acids	20.13	5.33
Isoquinoline		Alkaloids	24.81	1.74
Neophytadiene		Sesquiterpenoids (Terpenoids)	27.29	4.00
2-Pentadecanone, 6,10,14-trimethyl		Isopernoidal ketone	27.43	8.20
9,12-Octadecadienoic acid (Z,Z)		Fatty acids (Linoleic acid)	27.81	1.09
2,2-Dideutero octadecanal		Fatty acids	28.97	1.58
Hexadecanoic acid, ethyl ester $C_{18}H_{36}O_2$		Fatty acid (carboxylic acid esters)	30.43	3.24
Phytol		Terpenoids	32.68	1.96
Oleic Acid (9-Octadecenoic acid (Z)-)		Fatty acid	33.21	1.34
Octadecanoic acid, ethyl ester $C_{20}H_{40}O_2$		carboxylic acid esters	34.15	0.99
3',4',7-Trimethyl quercetin		Flavonoids	44.13	1.25
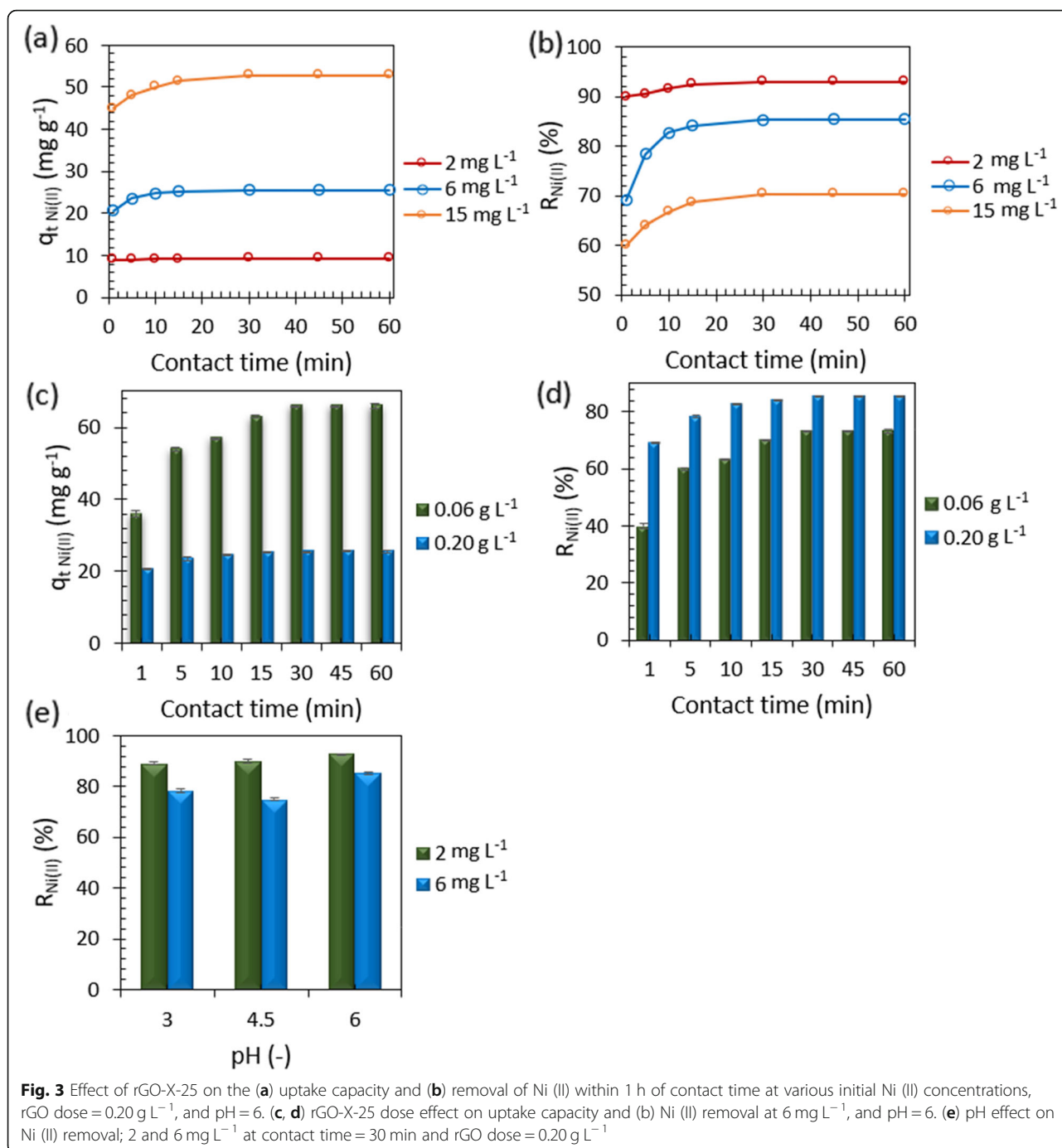
Fig. 3 Effect of rGO-X-25 on the (**a**) uptake capacity and (**b**) removal of Ni (II) within 1 h of contact time at various initial Ni (II) concentrations, rGO dose = 0.20 g L^{-1}, and pH = 6. (**c**, **d**) rGO-X-25 dose effect on uptake capacity and (b) Ni (II) removal at 6 mg L^{-1}, and pH = 6. (**e**) pH effect on Ni (II) removal; 2 and 6 mg L^{-1} at contact time = 30 min and rGO dose = 0.20 g L^{-1}

Table 4 illustrates the parameters of the isotherm and kinetics models based on non-linear equations. Non-linear models were preferred because of their achieving accurate variables and parameters for illustrating the adsorption process based on the previous work of Mahmoud [5].

The investigated isotherm models' constants associated with Eqs. (3)–(5) are the shown in Table 4. The Langmuir adsorption isotherm is related to the number

of active sites of the adsorbent in the adsorption process. The calculated q_m of rGO was 69 mg g^{-1} from the non-linear Langmuir model revealing the maximum adsorption uptake in monolayer of metal ions on the rGO sample surface. The value of K_L which equals 0.66 L mg^{-1}, indicates the affinity of the metal ion to the rGO adsorption sites. Our K_L value is higher than the reported one for Ni (II) adsorption using 0.2 g L^{-1} of Cloisite Na^+ clay at pH 7 ($K_L = 0.25$ L mg^{-1}) in Maleki and Karimi-Jashni

Fig. 4 Non-linear (**a**) isotherm and (**b**) kinetic models for Ni (II) removal using rGO-X-25. (**c**) Separation factor plot of rGO-X-25 for Ni (II) removal

[33]. The binding affinity between Ni (II) and rGO sample could be proven by the SF. Figure 4c illustrates the that the values of SF were found in the range of the range of 0–1 so the adsorption isotherm is favorable. When the values of SF are > 1 or = 1 or = 0, the adsorption isotherm is either unfavorable or linear or irreversible [5].

Temkin model assumes that the adsorption heat of adsorbate decreased with the increase in coverage of the adsorbent surface ignoring the extremely low and large value of concentrations. The application of Temkin model indicates the indirect adsorption heat of Ni (II) ions on rGO sample surface that reflects the surface coverage of rGO. The high values of R^2 and the values of error functions of the investigated models proved the suitability of those models for the description of Ni (II) adsorption using rGO at room temperature with the order of Freundlich, Langmuir, and Temkin. Freundlich isotherm designated that the heterogeneous surfaces of the rGO are applicable in the adsorption process.

Adsorption kinetics describes the rate of adsorbate retained or released from an aqueous solution to a solid-phase interface under various conditions. The order and rate kinetic constants of Ni (II) adsorption onto rGO sample could be determined by pseudo-first-order (PFO) or pseudo-second-order (PSO). Figure 4b shows the increment of Ni (II) uptake till the equilibrium was observed at 30 min. The uptake capacity of Ni (II) was high during the first 10 min due to the available adsorption sites of rGO sample. In the present account, Ni (II) adsorption rate constant was fitted to the PSO on the basis of $R^2 = 0.984$ as well as the error functions were the minimum compared to the PFO. PSO assumes that the rate of adsorption of the adsorbate is proportional to the available sites on the adsorbent [34].

3.4.3 RSM

Based on Eq. (10), the Ni (II) removal efficiency (R%) can be fitted by the following equation to relate between the factors and the response whatever their significance. Equation (13) can estimate the response and its accuracy is checked whether the model is adequate to predict.

$$\begin{aligned} R = {} & 68.89 + 7.24\,pH - 19.85\,Conc. + 7.66\,Dose \\ & + 4.52\,pH\,x\,Conc. - 1.37\,pH\,x\,Dose \\ & + 3.37\,Conc.x\,Dose + 1.44\,pH^2 \\ & + 3.49\,Conc.^2 - 3.64\,Dose^2 \end{aligned} \tag{13}$$

The factors could be synergistic or antagonistic effects as illustrated in Eq. (7). The factors (pH and Dose) possessed synergistic effects. It signifies that the increment of the pH and the rGO dose within the studied range improves the Ni (II) removal efficiency. Whereas the initial concentration effect (Conc.) had an antagonistic

Table 4 Nonlinear isotherm, kinetic parameters, regression coefficients and error functions for Ni (II) removal using rGO-X-25

Isotherm models	Parameters	Values	Kinetic models	Parameters	Values
Langmuir			Pseudo-first-order		
	$q_{m\,cal}$ (mg g^{-1})	69		$q_{e\,cal}$ (mg g^{-1})	25
	K_L (L mg^{-1})	0.66		k_1 (min^{-1})	1.7
	R^2	0.986		R^2	0.892
Error functions*			Error functions*		
	X^2	0.85		X^2	0.08
	SSE	9.77		SSE	1.64
	ARED	6.92		ARED	1.67
	MPSED	15.34		MPSED	2.36
Freundlich			Pesudo-second-order		
	K_f ((mg g^{-1}) (mg L^{-1})^n)	25.8		$q_{e\,cal}$ (mg g^{-1})	26
	n	0.51		k_2 (g mg^{-1} min^{-1})	0.16
	R^2	0.987		R^2	0.984
Error functions*			Error functions*		
	X^2	0.39		X^2	0.01
	SSE	13.73		SSE	0.27
	ARED	4.21		ARED	0.82
	MPSED	6.14		MPSED	0.96
Temkin					
	B	12.2			
	K_T (L mg^{-1})	12.4			
	R^2	0.963			
Error functions*					
	X^2	1.75			
	SSE	38.44			
	ARED	11.20			
	MPSED	18.09			

*X^2: chi-squared test, SSE: sum of the squares of errors, ARED: average relative error deviation, MPSED: Marquardt's percent standard error deviation

* $X^2 = \sum \frac{(q_{e,\,exp}-q_{e,cal})^2}{q_{e,cal}}, \cdot\ SSE = \sum (q_{e,\,exp}-q_{e,cal})^2\ \ ARED = \frac{1}{N}\sum |\frac{(q_{e,\,exp}-q_{e,\,exp})^2}{q_{e,\,exp}}|x\ 100,$

$MPSED = \sqrt{\frac{\sum [(q_{e,\,exp}-q_{e,cal})/q_{e,\,exp}]^2}{N-P}}x\ 100$

effect that the removal efficiency of Ni (II) is decreased with high Conc.

Optimization experimental design with the three factors and their responses are provided in Table S1. The maximum removal was determined 92.95% with optimum conditions of pH = 6, concentration of Ni (II) = 2 mg L^{-1}, and rGO dose = 0.2 g L^{-1}. The influence of these factors on the removal of Ni (II) was evaluated using ANOVA and its result are illustrated in Table S2. The model's F-value of 127 indicates that it is significant and F-value of this magnitude has 0.01% chance of occurring due to noise.

It is noting that the model factors are significant when *P*-values are < 0.05. Otherwise, the model factors will be not significant. In this case the three individual factors and the two-interaction factors are significant except for pH *x* Dose. It may be the response was largely increased or decreased with the interaction of pH *x* Dose.

In addition, Table S2 shows that R^2 was 0.994 to reveal the agreement between experimental and predicted values that implied the reliability of the developed model in the removal of Ni (II) from simulated wastewater. In literature studies, obtained the model R^2 with 0.989 that matched the predicted values and experimental values of Ni (II) adsorption on fungal-chitosan-magnetic magnetite nanocomposite [35]. Furthermore, it is noticeable that the adjusted and predicted R^2 are close to each other, and their difference is very small (0.030) so the BBD model is compatible. The value of "Adeq Precision" was 38.8 which indicates the desirability of the model when its ratio is more than 4 and reflects the adequate signal.

Figure 5a shows the random spots of the experimental data points in a range of − 4.8 and + 4.8 which implies that the proposed model was adequate and satisfied the
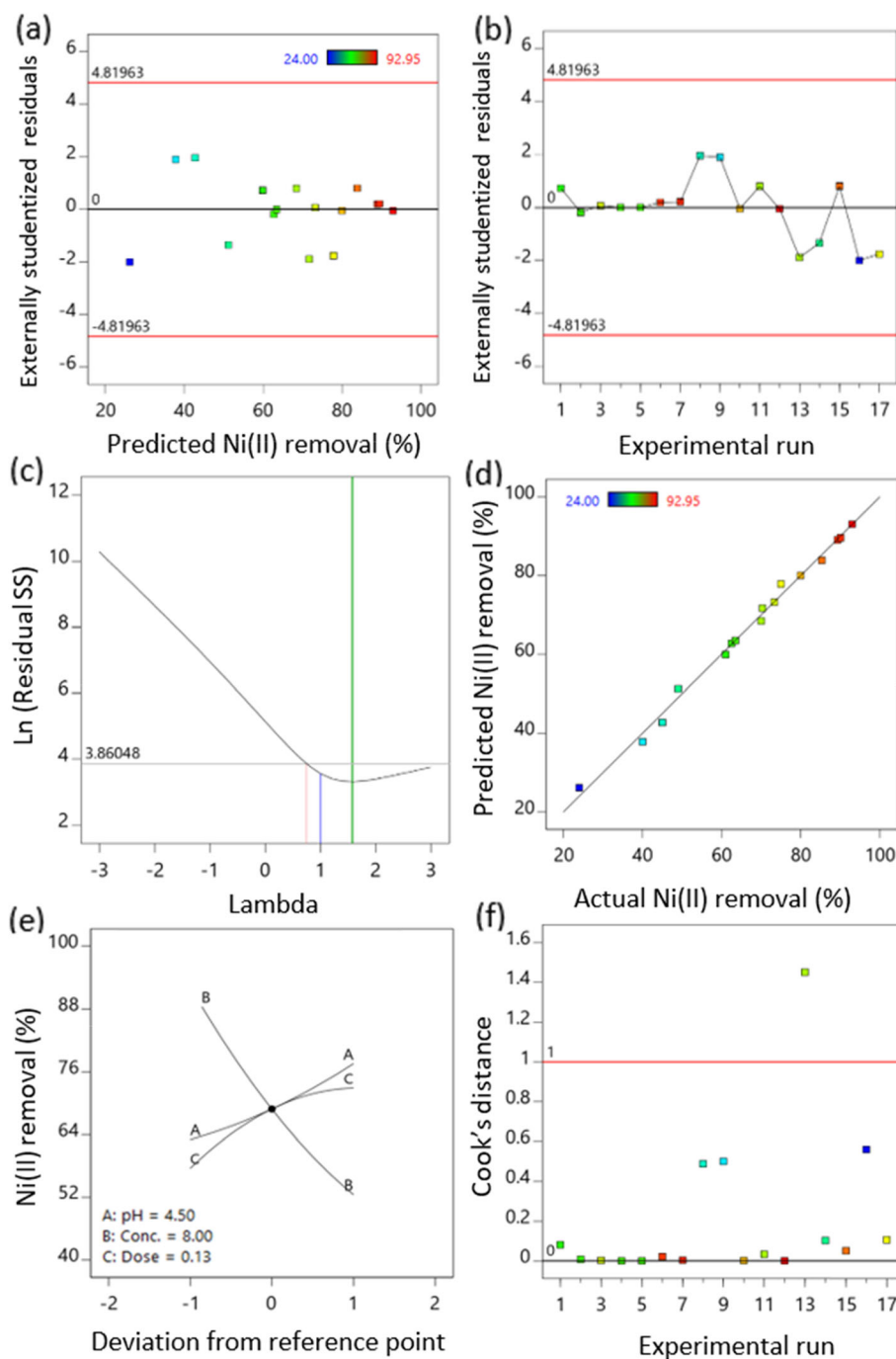
Fig. 5 Plots of externally studentized residuals with (**a**) predicted response; Ni (II) removal, (**b**) the number of runs in BBD design. (**c**) Box-Cox plot, (**d**) validation model by the relationship between predicted and actual values of the response. (**e**) The effect of perturbation of each process variable, (**f**) Cook's distance for each experimental run

assumption of constant variance as highlighted in Ghoreishian et al. [36]. This variance could be unchanged with the residual factors. Similar constant range of the experimental range between − 4 and + 4 was recorded in Ghoreishian et al. [37] who used rGO/CdWO$_4$ composite for sono-photocatalytic degradation.

The fitting proof of the model is also given in Fig. 5b where the data points are within the constant range and there is no specific trend. Such findings affirmed that the experimental data points were randomly scattered. The best lambda is found in the range of 0.75–3.25 at confidence level 95% as shown in Fig. 5c. It reveals that
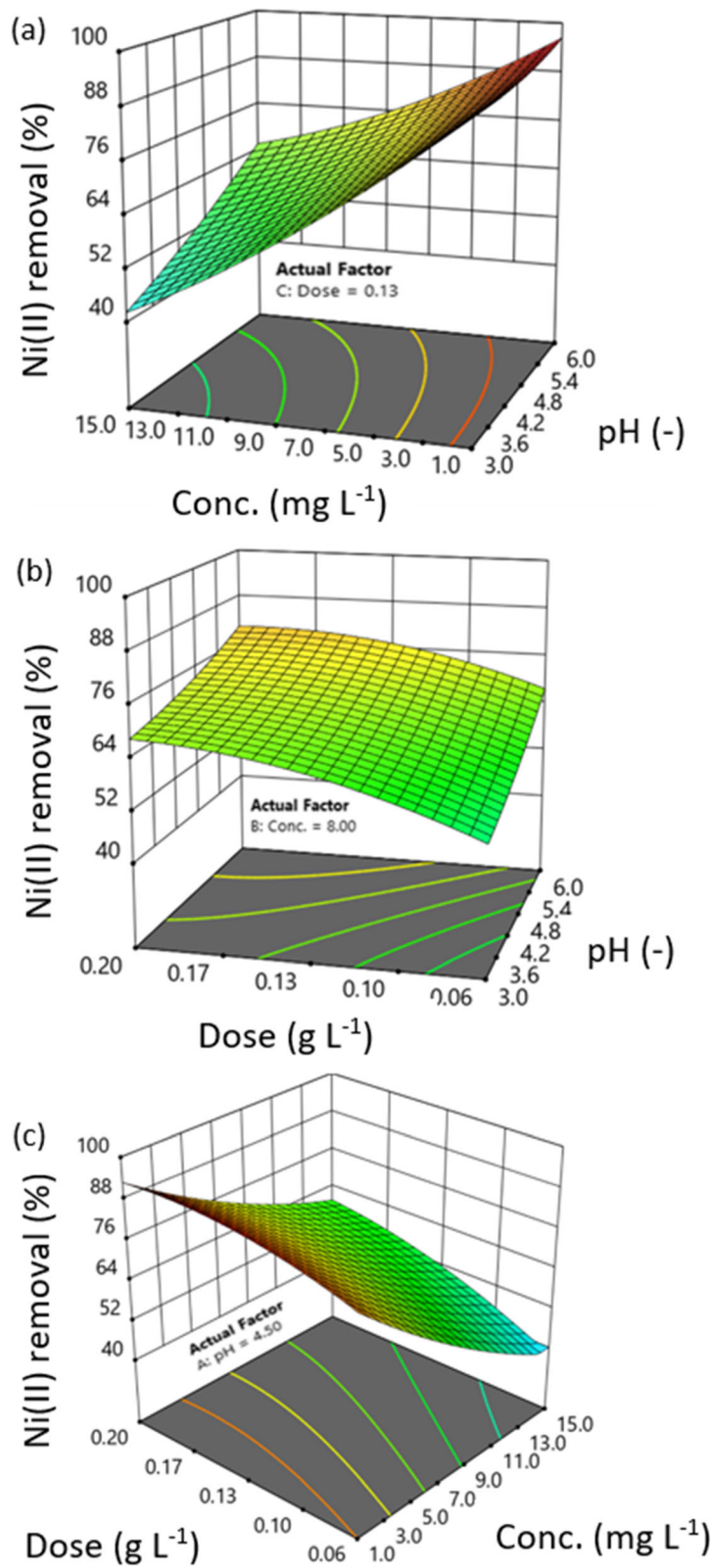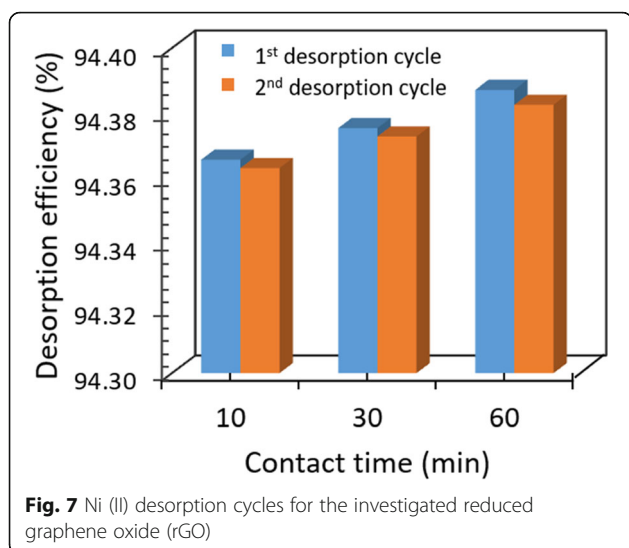
Fig. 6 3D response surface plots for Ni (II) removal using rGO with the interaction effects of (**a**) Ni (II) concentration (Conc.) *x* pH, (**b**) Dose *x* pH, and (**c**) Dose *x* Initial Ni (II) concentration (Conc.).

Fig. 7 Ni (II) desorption cycles for the investigated reduced graphene oxide (rGO)

no transformation of the response is needed as recommended by the software because the transformation is only needed if the residual errors are function of the predicted values magnitude. Figure 5d validates the close set of the predicted and the experimental values for Ni (II) removal process. This is illustrated through the distribution of the points close to the diametric line.

Figure 5e shows the impact of each factor effect on the Ni (II) removal around its reference point. The reference value of 4.5, 8 mg L^{-1}, and 0.13 g L^{-1} represent pH, Conc., and Dose, respectively. The behavior of each factor varies because of their interactive effect on the response. It is noting that the increment of pH (A) and Dose (C) above their reference points considerably enhanced the removal efficiency. On the other hand, the increment of Conc. (B) from its reference point resulted in high decreasing of the removal efficiency. These findings imply the sensitivity of the studied factors on the removal of Ni (II) using rGO.

It is noted that the cook's distances of most experimental runs are less than 1 and almost zero as illustrated in Fig. 5f except for run 13. Such finding proves the efficiency of the model in prediction. All aforementioned

values are tabulated in the supplementary information (Table S3).

3.5 Parameters affecting the removal of Ni (II)
The 3D response surfaces of Ni (II) removal models using rGO are illustrated in Fig. 6a-c. The produced plots are a result of two interactive variables while keeping the third variable constant at the center point. The intensity of the variable interactions is depicted by the curvature of those plots [38]. The surface plots reveal the significance of the studied factors on the Ni (II) removal models using rGO.

The decrement of initial Ni (II) concentration with increasing pH values resulted in high Ni (II) removal (Fig. 6a). The Ni (II) removal reached 96% with 1 mg L^{-1}, pH of 6, and rGO dose of 0.13 g L^{-1}. This could be related to the rGO surface area available for Ni (II) removal at low concentration and the negatively charged surface of rGO [5, 14]. When initial Ni (II) concentration is fixed at 8 mg L^{-1}, its removal efficiency was 80% at pH of 6 and rGO dose of 0.2 g L^{-1} (Fig. 6b). Despite the Ni (II) removal is not dramatically changed with pH values (3–6) as shown earlier in OFAT, its removal is low at lower pH because of the metal restriction approach from the repulsive force between the adsorbent and the metal ions and decreasing the adsorption process [39]. Figure 6c illustrates the enhancement of Ni (II) removal from 84 to 93% with the increment of rGO dose from 0.06 to 0.20 g L^{-1}.

3.6 Desorption and reusability of rGO
The applicability of utilizing rGO in successive cycles for the removal of Ni (II) was assessed through the investigation of rGO desorption efficiency. The desorption of Ni (II) on rGO was done using a desorption agent (0.1 M HNO$_3$). Fig. 7 shows two consecutive desorption cycles with different treatment time. The average desorption of Ni (II) was 94%. It is observed that the results are close enough with different treatment time so the desorption process can be conducted at 10 min. The efficiency of the second cycle was decreased than the first one because the desorption agent affected the adsorption sites.

Table 5 Ni (II) adsorption capacity stated in literature studies compared to the present study

Adsorbent	pH (–)	Concentration (mg L^{-1})	Time (min)	Maximum adsorption capacity (mg g^{-1})	References
Reduced graphene oxide (rGO)	6	2	30	69	This study
Magnetic graphene oxide	7	60	25	51	[26]
Graphene oxide	8	350	270	102	[27]
Manganese ferrite-graphene oxide nanocomposite	8	350	270	152	
Magnetite graphene oxide-chitosan nanocomposite	–	135	70	12	[42]
Graphene oxide-almond shell composite	7.5	200	180	69	[43]

Akhayere et al. [40] found the sorption efficiency of Ni (II) after many desorption cycles at 95–91% and 82–77% with barley-nanosilica and wheat-nanosilica, respectively using acetic acid as a solvent. On the other hand, Le et al. [41] stated a low efficiency of Ni removal (27%) after five cycles using EDTA as a washing solution because of reducing active bonding sites of magnetic composite with GO and chitosan beads that were employed as an adsorbent in the acidic environment.

3.7 Comparison to literature

When a comparison was drawn among various adsorbents that were utilized for the removal of Ni (II) from simulated wastewater, it was concluded that the maximum adsorption capacity of our green synthesized rGO prepared in this work was higher with short contact time than most of the recorded capacities of other adsorbents in literature. Although few sorbents were found higher in the adsorption capacity than the used sorbent, they need long contact time with higher pH. Table 5 lists various reported experimental conditions compared to our studied conditions.

4 Conclusions

In this work, graphene oxide was successfully reduced to reduced graphene oxide using the leaves extracts of *T. stans*. It is confirmed by the rGO characteristic peaks at ∼ 280 nm as well as the findings of FT-IR revealing that plant extracts had the capacity to reduce the oxygen functional groups on the GO surface. The O:C ratios of the prepared rGOs intensely plummeted after the reduction process in the following order: rGO-X-5 (0.46) > rGO-X-25 (0.38) > rGO-X-50 (0.35) The synthesized rGO-X-25 was chosen as the optimum product of rGOs due to its corrugated and wrinkled shape. It was applicable to remove Ni (II) from aqueous solutions as an adsorbent. The occurrence of adsorption process was verified by the appearance of Ni (II) peak in EDX analysis. Non-linear models and response surface area methodology were applied to Ni (II) adsorption. The q_m of Ni (II) was 69 mg g^{-1} and the adsorption rate was fitted to the pseudo-second-order with nonlinear models on the basis of $R^2 = 0.984$ as well as the low values of the error functions. The optimum removal of 2 mg L^{-1} Ni (II) was determined 93% under the conditions; pH of 6 and rGO dose of 0.2 g L^{-1} while the Ni (II) removal reached 96% at 1 mg L^{-1}, pH of 6, and rGO dose of 0.13 g L^{-1}. Furthermore, the synthesized rGO showed high desorption efficiency for multiple usages. Based on the findings, rGO possesses promising capabilities for Ni (II) removal with possible reusability. Hence, it is recommended to test rGO with other metal ions present in wastewater.

5 Supplementary Information

The online version contains supplementary material available at https://doi.org/10.1186/s42834-022-00131-0.

> **Additional file 1.**

Authors' contributions
Alaa El Din Mahmoud: investigated, provided conceptualization, methodology, visualization, processed formal analysis, project administration, and acquisition of funding as well as conducting writing-original draft preparation and writing-review & editing. Mohamed Hosny: investigated, provided methodology and conducting writing-original draft preparation. Nourhan El-Maghrabi: investigated and provided methodology. Manal Fawzy: provided supervision, resources, and conducting writing—review & editing. All authors read and approved the final manuscript.

Availability of data and materials
All data generated or analyzed during this study are available from the corresponding author on reasonable request.

Declarations

Competing interests
The authors declare that they have no competing financial interests that could have appeared to influence the work reported in this paper.

Author details
[1]Environmental Sciences Department, Faculty of Science, Alexandria University, Alexandria 21511, Egypt. [2]Green Technology Group, Alexandria University, Alexandria 21511, Egypt. [3]National Egyptian Biotechnology Experts Network, National Egyptian Academy for Scientific Research and Technology, Cairo 11516, Egypt.

References

1. El Din Mahmoud A, Fawzy M. Bio-based methods for wastewater treatment: green sorbents. In: Ansari AA, Gill SS, Gill R, Lanza GR, Newman L, editors. Phytoremediation. Cham: Springer; 2016. p. 209–38.
2. Ali H, Khan E. Trophic transfer, bioaccumulation, and biomagnification of non-essential hazardous heavy metals and metalloids in food chains/webs—Concepts and implications for wildlife and human health. Hum Ecol Risk Assess. 2019;25:1353–76.
3. Nandi D, Saha I, Ray SS, Maity A. Development of a reduced-graphene-oxide based superparamagnetic nanocomposite for the removal of nickel (II) from an aqueous medium via a fluorescence sensor platform. J Colloid Interface Sci. 2015;454:69–79.
4. Alkafajy AM, Albayati TM. High performance of magnetic mesoporous modification for loading and release of meloxicam in drug delivery implementation. Mater Today Commun. 2020;23:100890.
5. Mahmoud AED. Graphene-based nanomaterials for the removal of organic pollutants: insights into linear versus nonlinear mathematical models. J Environ Manag. 2020;270:110911.
6. Mahmoud AED, Al-Qahtani KM, Alflaij SO, Al-Qahtani SF, Alsamhan FA. Green copper oxide nanoparticles for lead, nickel, and cadmium removal from contaminated water. Sci Rep 2021;11:12547.
7. Yap PL, Tung TT, Kabiri S, Matulick N, Tran DNH, Losic D. Polyamine-modified reduced graphene oxide: a new and cost-effective adsorbent for efficient removal of mercury in waters. Sep Purif Technol. 2020;238:116441.

8. Mahmoud AED. Eco-friendly reduction of graphene oxide via agricultural byproducts or aquatic macrophytes. Mater Chem Phys. 2020;253:123336.

9. Weng XL, Wu J, Ma L, Owens G, Chen ZL. Impact of synthesis conditions on Pb (II) removal efficiency from aqueous solution by green tea extract reduced graphene oxide. Chem Eng J. 2019;359:976–81.

10. Anand M, Basavaraju R. A review on phytochemistry and pharmacological uses of *Tecoma stuns* (L.) Juss. ex Kunth. J Ethnopharmacol. 2021;265: 113270.

11. Hariram M, Vivekanandhan S, Ganesan V, Muthuramkumar S, Rodriguez-uribe A, Mohanty AK, et al. Tecoma stans flower extract assisted biogenic synthesis of functional Ag-Talc nanostructures for antimicrobial applications. Bioresour Technol Rep. 2019;7:100298.

12. Nguyen DTC, Dang HH, Vo DVN, Bach LG, Nguyen TD, Tran TV. Biogenic synthesis of MgO nanoparticles from different extracts (flower, bark, leaf) of *Tecoma stans* (L.) and their utilization in selected organic dyes treatment. J Hazard Mater. 2021;404:124146.

13. Mahmoud AED, Fawzy M, Hosny G, Obaid A. Equilibrium, kinetic, and diffusion models of chromium (VI) removal using *Phragmites australis* and *Ziziphus spina-christi* biomass. Int J Environ Sci Technol. 2021;18:2125–36.

14. Mahmoud AED, Fawzy M, Radwan A. Optimization of Cadmium (CD^{2+}) removal from aqueous solutions by novel biosorbent. Int J Phytoremediat. 2016;18:619-25.

15. Ansari MZ, Johari R, Siddiqi WA. Novel and green synthesis of chemically reduced graphene sheets using *Phyllanthus emblica* (Indian Gooseberry) and its photovoltaic activity. Mater Res Express. 2019;6:055027.

16. Neolaka YAB, Lawa Y, Naat JN, Riwu AAP, Iqbal M, Darmokoesoemo H, et al. The adsorption of Cr (VI) from water samples using graphene oxide-magnetic (GO-Fe$_3$O$_4$) synthesized from natural cellulose-based graphite (kusambi wood or *Schleichera oleosa*): study of kinetics, isotherms and thermodynamics. J Mater Res Technol. 2020;9:6544–56.

17. Emadi F, Amini A, Gholami A, Ghasemi Y. Functionalized graphene oxide with chitosan for protein nanocarriers to protect against enzymatic cleavage and retain collagenase activity. Sci Rep UK. 2017;7:42258.

18. Kumar TR, Yoo DJ, Kim AR, Kumar GG. Green synthesis of Pt-Pd bimetallic nanoparticle decorated reduced graphene oxide and its robust catalytic activity for efficient ethylene glycol electrooxidation. New J Chem. 2018;42: 14386–93.

19. Vatandost E, Ghorbani-HasanSaraei A, Chekin F, Raeisi SN, Shahidi SA. Green tea extract assisted green synthesis of reduced graphene oxide: application for highly sensitive electrochemical detection of sunset yellow in food products. Food Chem X. 2020;6:100085.

20. Ding ZY, Yuan TQ, Wen JL, Cao XF, Sun SN, Xiao LP, et al. Green synthesis of chemical converted graphene sheets derived from pulping black liquor. Carbon. 2020;158:690–7.

21. Kurmarayuni CM, Kurapati S, Akhil S, Chandu B, Khandapu BMK, Koya PR, et al. Synthesis of multifunctional graphene exhibiting excellent sonochemical dye removal activity, green and regioselective reduction of cinnamaldehyde. Mater Lett. 2020;263:127224.

22. Ahmad S, Ahmad A, Khan S, Ahmad S, Khan I, Zada S, et al. Algal extracts based biogenic synthesis of reduced graphene oxides (rGO) with enhanced heavy metals adsorption capability. J Ind Eng Chem. 2019;72:117–24.

23. Coros M, Pogacean F, Turza A, Dan M, Berghian-Grosan C, Pana IO, et al. Green synthesis, characterization and potential application of reduced graphene oxide. Phys E. 2020;119:113971.

24. Larbie C, Nyarkoh CO, Adjei CO. Phytochemical and safety evaluation of hydroethanolic leaf extract of *Tecoma stans* (L.) Juss. ex Kunth. Evid Based Compl Alt. 2019;2019:7417624.

25. Xiao XF, Wang Q, Owens G, Chiellini F, Chen ZL. Reduced graphene oxide/ iron nanoparticles used for the removal of Pb (II) by one step green synthesis. J Colloid Interface Sci. 2019;557:598–607.

26. Ain QU, Farooq MU, Jalees MI. Application of magnetic graphene oxide for water purification: heavy metals removal and disinfection. J Water Process Eng. 2020;33:101044.

27. Thy LTM, Kiem NH, Tu TH, Phu LM, Oanh DTY, Nam HM, et al. Fabrication of manganese ferrite/graphene oxide nanocomposites for removal of nickel ions, methylene blue from water. Chem Phys. 2020;533:110700.

28. Ghodke SA, Maheshwari U, Gupta S, Sonawane SH, Bhanvase BA. Nanomaterials for adsorption of pollutants and heavy metals: introduction, mechanism, and challenges. In: Bhanvase B, Sonawane S, Pawade V, Pandit A, editors. Handbook of nanomaterials for wastewater treatment. Amsterdam: Elsevier; 2021. p. 343–66.

29. Mahmoud AED, Franke M, Stelter M, Braeutigam P. Mechanochemical versus chemical routes for graphitic precursors and their performance in micropollutants removal in water. Powder Technol. 2020;366:629–40.

30. Ma JZ, Hou LY, Li P, Zhang SM, Zheng XY. Modified fruit pericarp as an effective biosorbent for removing azo dye from aqueous solution: study of adsorption properties and mechanisms. Environ Eng Res. 2021;27:200634.

31. Naeemullah, Tuzen M, Sari A, Turkekul I. Influential bio-removal of mercury using Lactarius acerrimus macrofungus as novel low-cost biosorbent from aqueous solution: isotherm modeling, kinetic and thermodynamic investigations. Mater Chem Phys. 2020;249:123168.

32. Eftekhari M, Akrami M, Gheibi M, Azizi-Toupkanloo H, Fathollahi-Fard AM, Tian GD. Cadmium and copper heavy metal treatment from water resources by high-performance folic acid-graphene oxide nanocomposite adsorbent and evaluation of adsorptive mechanism using computational intelligence, isotherm, kinetic, and thermodynamic analyses. Environ Sci Pollut R. 2020;27:43999–4021.

33. Maleki S, Karimi-Jashni A. Optimization of Ni (II) adsorption onto Cloisite Na$^+$ clay using response surface methodology. Chemosphere. 2020;246:125710.

34. Kadhum ST, Alkindi GY, Albayati TM. Eco friendly adsorbents for removal of phenol from aqueous solution employing nanoparticle zero-valent iron synthesized from modified green tea bio-waste and supported on silty clay. Chin J Chem Eng. 2021;36:19–28.

35. Ince OK, Aydogdu B, Alp H, Ince M. Experimental design approach for ultra-fast nickel removal by novel bio-nanocomposite material. Adv Nano Res. 2021;10:77–90.

36. Ghoreishian SM, Norouzi M, Fereydooni A, Nasser S, Asadolahi T, Beigpour N, et al. Optimization of melt-spinning parameters of poly (ethylene terephthalate) partially oriented multi-filament yarn in an industrial scale: central composite design approach. Fiber Polym. 2017;18:1280–7.

37. Ghoreishian SM, Raju GSR, Pavitra E, Kwak CH, Han YK, Huh YS. Ultrasound-assisted heterogeneous degradation of tetracycline over flower-like rGO/ CdWO$_4$ hierarchical structures as robust solar-light-responsive photocatalysts: optimization, kinetics, and mechanism. Appl Surf Sci. 2019; 489:110–22.

38. Lingamdinne LP, Koduru JR, Chang YY, Karri RR. Process optimization and adsorption modeling of Pb (II) on nickel ferrite-reduced graphene oxide nano-composite. J Mol Liq. 2018;250:202–11.

39. Davarnejad R, Panahi P. Cu (II) and Ni (II) removal from aqueous solutions by adsorption on Henna and optimization of effective parameters by using the response surface methodology. J Ind Eng Chem. 2016;33:270–5.

40. Akhayere E, Essien EA, Kavaz D. Effective and reusable nano-silica synthesized from barley and wheat grass for the removal of nickel from agricultural wastewater. Environ Sci Pollut R. 2019;26:25802–13.

41. Le TTN, Le VT, Dao MU, Nguyen QV, Vu TT, Nguyen MH, et al. Preparation of magnetic graphene oxide/chitosan composite beads for effective removal of heavy metals and dyes from aqueous solutions. Chem Eng Commun. 2019;206:1337–52.

42. Tran LT, Tran HV, Le TD, Bach GL, Tran LD. Studying Ni (II) adsorption of magnetite/graphene oxide/chitosan nanocomposite. Adv Polym Technol. 2019;2019:8124351 .

43. Moghaddam NY, Lorestani B, Cheraghi M, Jamehbozorgi S. Adsorption of Cd and Ni from water by graphene oxide and graphene oxide-almond shell composite. Water Environ Res. 2019;91:475–82.

Publisher's Note